

---

**Research Article: New Research | Novel Tools and Methods**

## **Selective activation of resting state networks following focal stimulation in a connectome-based network model of the human brain**

Stimulation in connectome-based brain models

**Andreas Spiegler<sup>1</sup>, Enrique C.A. Hansen<sup>1</sup>, Christophe Bernard<sup>1</sup>, Anthony R. McIntosh<sup>2</sup> and Viktor K. Jirsa<sup>1</sup>**

<sup>1</sup>*Institut de la Santé et de la Recherche Médicale, Aix Marseille Université, Institut de Neurosciences des Systèmes UMR\_S 1106, 13005, Marseille, France*

<sup>2</sup>*Rotman Research Institute of Baycrest Center, University of Toronto, Toronto, M6A 2E1, Canada*

DOI: 10.1523/ENEURO.0068-16.2016

Received: 23 March 2016

Revised: 7 June 2016

Accepted: 27 June 2016

Published: 21 September 2016

---

**Author Contributions:** AS and VKJ Designed Research; AS Performed Research; AS, ECAH, ARM, VKJ Contributed Tools; AS, ECAH Analyzed Data; AS, ECAH, CB, ARM, VKJ Wrote the paper.

**Funding:** James S. McDonnell Foundation, Brain Network Recovery Group

**Funding:** European Union Seventh Framework Programme: FP7-ICT Human Brain Project

**Conflict of Interest:** Authors report no conflict of interest.

James S. McDonnell Foundation and the European Union Seventh Framework Programme.

**Correspondence should be addressed to** Andreas Spiegler, Email: [andreas.spiegler@univ-amu.fr](mailto:andreas.spiegler@univ-amu.fr)

**Cite as:** eNeuro 2016; 10.1523/ENEURO.0068-16.2016

**Alerts:** Sign up at [eneuro.org/alerts](http://eneuro.org/alerts) to receive customized email alerts when the fully formatted version of this article is published.

Accepted manuscripts are peer-reviewed but have not been through the copyediting, formatting, or proofreading process.

This is an open-access article distributed under the terms of the Creative Commons Attribution 4.0 International (<http://creativecommons.org/licenses/by/4.0>), which permits unrestricted use, distribution and reproduction in any medium provided that the original work is properly attributed.

Copyright © 2016 the authors

1 **1. Manuscript Title** Selective activation of resting state networks following focal stimulation in  
2 a connectome-based network model of the human brain

3 **2. Abbreviated Title** Stimulation in connectome-based brain models

4 **3. Author Names and Affiliations** Andreas Spiegler<sup>1</sup>, Enrique C.A. Hansen<sup>1</sup>, Christophe  
5 Bernard<sup>1</sup>, Anthony R. McIntosh<sup>2</sup>, Viktor K. Jirsa<sup>1</sup>

6 <sup>1</sup>Aix Marseille Université, Institut de la Santé et de la Recherche Médical, Institut de  
7 Neurosciences des Systèmes UMR\_S 1106, 13005, Marseille, France

8 <sup>2</sup>Rotman Research Institute of Baycrest Center, University of Toronto, Toronto, M6A 2E1,  
9 Canada

10 **4. Author Contributions:** AS and VKJ Designed Research; AS Performed Research; AS, ECAH,  
11 ARM, VKJ Contributed Tools; AS, ECAH Analyzed Data; AS, ECAH, CB, ARM, VKJ Wrote  
12 the paper

13 **5. Correspondence should be addressed to** andreas.spiegler@univ-amu.fr

14 **6. Number of Figures** 7 **9. Number of words for Abstract** 227

15 **7. Number of Tables** 2 **10. Number of words for Significance Statement** 94

16 **8. Number of Multimedia** 0 **11. Number of words for Introduction** 692

17 **12. Number of words for Discussion** 3035

18 **13. Acknowledgements** The research reported herein was supported by the Brain Network  
19 Recovery Group through the James S. McDonnell Foundation and funding from the European  
20 Union Seventh Framework Programme: FP7-ICT Human Brain Project (grant no. 60 402).

21 **14. Conflict of Interest:** The authors declare no competing financial interests.

22 **15. Funding sources:** James S. McDonnell Foundation and the European Union Seventh  
23 Framework Programme

**Abstract**

24 When the brain is stimulated, for example, by sensory inputs or goal-oriented tasks, the brain  
25 initially responds with activities in specific areas. The subsequent pattern formation of functional  
26 networks is constrained by the structural connectivity (SC) of the brain. The extent to which  
27 information is processed over short- or long-range SC is unclear. Whole-brain models based on  
28 long-range axonal connections, for example, can partly describe measured functional  
29 connectivity dynamics at rest. Here, we study the effect of SC on the network response to  
30 stimulation. We use a human whole-brain network model comprising long- and short-range  
31 connections. We systematically activate each cortical or thalamic area, and investigate the  
32 network response as a function of its short- and long-range SC. We show that when the brain is  
33 operating at the edge of criticality, stimulation causes a cascade of network recruitments,  
34 collapsing onto a smaller space that is partly constrained by SC. We found both short- and long-  
35 range SC essential to reproduce experimental results. In particular, the stimulation of specific  
36 areas results in the activation of one or more resting state networks. We suggest that the stimulus-  
37 induced brain activity, which may indicate information and cognitive processing, follows specific  
38 routes imposed by structural networks explaining the emergence of functional networks. We  
39 provide a lookup table linking stimulation targets and functional network activations, potentially  
40 useful in diagnostics and treatments with brain stimulation.

**Significance Statement**

41 Systematic exploration via stimulation of all cortical and subcortical brain areas can only be  
42 performed *in silico*. We have performed a detailed parametric exploration of dynamically  
43 responsive networks of a large-scale brain network model to stimulation and developed a  
44 stimulation map indicating which brain areas need to be stimulated to place the brain in a  
45 particular state at rest. Brain stimulation is one of the upcoming novel tools in the treatment of

46 neurological disorders. The stimulation map will be critical in guiding these studies and allow for  
47 the development of theory guided stimulation protocols.

## Introduction

Sensory stimulation is important to understand perception and information processing in the brain.

To study cognitive functions, direct stimulation techniques, such as transcranial magnetic stimulation (TMS) and transcranial electrical stimulation (tES), are increasingly used. Moreover, direct brain stimulation is promising for treating psychiatric and neurological disorders (Parkin et al., 2015). Effects of direct stimulation are short-range, that is, local in a brain region, and long-range, that is, on a large-scale network. Both are important to understand the final outcome of the stimulation (Fox et al., 2014). There is however scant knowledge regarding the way of stimulating the brain to cause a predictable and beneficial effect. A conceptual framework is missing. Furthermore, the extent to which information is processed over short- or long-ranges is unclear.

Brain structures bear dynamics that give rise to diverse function and dysfunction (e.g., Park and Friston, 2013). Because structural connectivity (SC) constrains functional networks (e.g., Deco et al., 2015), we predict that stimulating a given area will give rise to a process of activity ultimately resolving in spatial patterns resembling functionally related networks. For example, direct stimulation of a primary sensory structure (e.g., the nucleus geniculatus lateralis thalami for the visual pathway) should cause responsive networks similar to those activated by a (visual) sensory input. The stimulation site of a responsive network can be part of (i) functional networks in which information is processed, (ii) ascending paths of sensory inputs, and (iii) structures modulating the information processing. Testing this hypothesis experimentally is delicate, as it requires knowing where and how to stimulate. The effect of stimulation of various cortical and subcortical brain areas can be systematically explored in silico.

Here, we use The Virtual Brain (TVB) platform, which allows studying dynamics in whole-brain models (Sanz-Leon et al., 2013, 2015), to systematically stimulate every area in the network

comprising long- and short-range SC (i.e., between brain areas and within an area), detect the responsive networks, and then contrast these to experimentally known networks, especially the resting state (RS-) networks (Damoiseaux et al., 2006). RS-networks describe, in the absence of external inputs or goal-oriented tasks, the consistent spatial patterns in the fluctuations of the BOLD signal (functional MRI). Furthermore, these patterns have been correlated to functionally related brain regions (i.e., active during task conditions) and have been called visual, memory, attention RS-networks etc. However, the link between the RS-networks and the functional networks occurring due to external stimuli or during goal-oriented tasks is not clear. The RS-networks, moreover, correlate with the SC of white matter tracts (van den Heuvel et al., 2009; Greicius et al., 2009; Hermundstad et al., 2013), thus appear as simple reflections of the large-scale network topology.

Local and global computation in the brain strongly depends upon short-range and long-range structural connections (Deco et al., 2015). We are taking into account both types of SC in TVB. Previous large-scale network model studies mostly considered long-range SC (i.e., white matter tracts). We go beyond this and incorporate short-range SC to understand how activity propagates and dissipates in the brain (Qubbaj and Jirsa, 2007, 2009; Jirsa, 2004; Jirsa and Kelso, 2000).

Large-scale brain networks have specific constraints due to the spatiotemporal scale of operation. Firstly, the time delays due to signal transmission via long white matter tracts between connecting nodes in brain network dynamics play a crucial role, for instance, in the generation of ongoing activity (Ghosh et al., 2008). Secondly, the connection strength, when scaled appropriately, places the brain close to criticality where the capacity of processing information is maximized and the functional connectivity best fits to empirical RS-data (Deco et al., 2014a; Deco and Jirsa, 2012; Ghosh et al., 2008). Finally, random processes serve to provide the brain

model with kinetic energy to form and alter functional networks (Hansen et al., 2015; Deco et al., 2014a; Ghosh et al., 2008).

Using an unbiased and deterministic approach, here we demonstrate that the large-scale brain network response to stimulation with functionally relevant activity patterns, which resemble the experimentally known RS-networks. In particular, we show that stimulation at spatially distant sites can give rise to similar non-stationary trajectories, whereas stimulation at spatially close sites can result in distinctly different dynamics.

### Materials and methods

48 Using *The Virtual Brain* platform (Sanz-Leon et al., 2013, 2015), we triangulate the surface of  
49 the cortex with a mesh of 8,192 nodes for each hemisphere (**Fig. 1a**), distributed across 74  
50 cortical areas (**Fig. 1b**), each containing between 29 and 683 nodes (Table 1), following a known  
51 functional parcellation atlas (Kötter and Wanke, 2005). The model also includes non-parcellated  
52 116 subcortical areas. To connect nodes with each other, we distinguish homogeneous from  
53 heterogeneous SC (**Fig. 1c–e**). The homogenous SC (of short-range connections) links nodes  
54 within an area, and between areas if they are spatially close from one another with a connection  
55 probability decreasing with distance (Braitenberg and Schüz, 1991) (**Fig. 1c**, and **d**). The  
56 heterogeneous SC (of long-range white matter tracts) links all the nodes of an area with the nodes  
57 of another area (**Fig. 1c and e**), based on known anatomical data (Kötter and Wanke, 2005).  
58 Neighboring areas are able to exchange information via the homogeneous SC within the cortex  
59 and via the white matter tract, that is, heterogeneous SC (e.g. Area 2 with Areas 1 and 3 in **Fig.**  
60 **1c**).  
61 Each vertex point is a network node holding a neural mass model connected to other nodes via  
62 the homogeneous SC and heterogeneous SC. When an area is stimulated, all the nodes of this  
63 area are simultaneously activated and then the stimulation-induced activity in each node decays

64 differently according to the activity in the surrounding via short-range connections (i.e.,  
65 homogeneous SC) and remote nodes via long-range connections (i.e., heterogeneous SC). The  
66 ability to drive the network does not depend on the number of nodes within an area, because the  
67 heterogeneous SC transfers the mean of the activity in all the nodes within an area to all the  
68 nodes in another areas.

69 We consider this ratio of homogeneous SC to heterogeneous SC as a degree of freedom and  
70 perform a parametric study (see Jirsa and Kelso, 2000; Qubbaj and Jirsa, 2007, 2009 for  
71 systematic studies with two-point connection). The ratio has been estimated. For instance,  
72 Braitenberg and Schüz (1998) assessed that pyramidal cells have synapses in equal shares from  
73 long-range and local axons. However, the ratio of homogeneous SC to heterogeneous SC mainly  
74 depends on the resolution of the used geometrical model of the cortex, with that the  
75 representation of the SC, and the network node description (e.g., canonical model, neural mass  
76 model), which is able to incorporate local connectivity (see, for example, Spiegler and Jirsa, 2013  
77 for more detail). At the extremes, (i) 0 % of heterogeneous SC (thus 100 % of homogeneous SC  
78 gives two unconnected cerebral hemispheres with locally but homogeneously connected nodes)  
79 only allows activity to propagate locally from a cortical stimulation site, and (ii) 100 % of  
80 heterogeneous SC (thus 0 % of homogenous SC gives 190 purely heterogeneously connected  
81 brain areas with locally unconnected nodes) only allows activity to travel long distances with  
82 time delays via white matter fiber tracts.

83 Furthermore, since the spatial range of homogeneous SC is not known (Spiegler and Jirsa, 2013),  
84 we also consider it as a parameter varying between 10 mm and 41 mm. We then systematically  
85 stimulate each of the 190 areas with a large range of parameter values (for the ratio and the  
86 spatial range), resulting in a total of all 37,620 simulation trials.



87 Brain dynamics at rest have been found to operate near criticality (Ghosh et al., 2008; Deco et al.,  
88 2011, 2013). Near-criticality is defined as a system that is on the brink of a qualitative change in  
89 its behavior (Shew and Plenz, 2013). The proximity to criticality predicts that the brain's  
90 response to stimulation will primarily arise from structures and networks that are closest to  
91 instability. Activities in those networks require the most time to settle into equilibria after  
92 stimulation, and are associated with large-scale dependencies and scale invariance (Haken, 1978).  
93 This would be consistent with the center manifold theorem, which states that a high-dimensional  
94 system in a subcritical state will converge on a lower dimensional manifold (here few networks)  
95 when the system is stimulated. Consequently, we equally set each node in the brain network  
96 model to operate close to its critical point, where the network shows no activity without  
97 stimulation. We use the stable regimen of each network node (i.e., stable focus) to stimulate a  
98 given area in the direction of its instability point (i.e., supercritical Andronov-Hopf bifurcation)  
99 and induce characteristic energy dissipation through the brain network. The dissipation of energy  
100 will be constrained by the homogeneous SC and heterogeneous SC, the associated signal  
101 transmission delays, and the local dynamics at the network nodes. In the network model, the  
102 operating point of every node, when disconnected from the network, is at the same distance from  
103 its critical point, that is, the supercritical Andronov-Hopf bifurcation (**Fig. 2a**). If the critical  
104 point is reached, the node enters into a constant oscillatory mode. In the network, the SC (incl.  
105 time delays) determine the alteration of the working distance to the critical point at each node in  
106 time by weighting and delaying the incoming activity from other nodes in the network. Hence,  
107 network metrics of the SC such as the in-strength, that is, the sum of weights of incoming ties to a  
108 node may indicate the distance of a node's operating point to its critical point and thus criticality  
109 (Kunze et al., 2016). The network model, however, is set so that criticality is never reached, by  
110 normalizing the SC to unity maximum in-strength so that activity cannot be amplified through the

111 SC. As a result, when a node is stimulated, the node operates closer to the critical point and the  
112 response is in the form of a damped oscillation (**Fig. 2a**). The closer a node operates to the  
113 critical point, the stronger the node's responses with high amplitude and long decay time (**Fig.**  
114 **2a**). The nodes are working near criticality (i.e., they get close to a change in behavior, which  
115 would be here a switch to a constant oscillatory mode, but never reaching it). Thus the response  
116 to the stimulation is transient, lasting a few milliseconds. The damped oscillation generated in  
117 one stimulated node is then sent via its efferent connections to its target nodes, triggering there, in  
118 turn, a damped oscillation (**Fig. 2b**). If the network were mainly based on nodes connected in  
119 series, activity would decay very fast after the stimulation (**Fig. 2b**). However, since the outgoing  
120 activity of a node can influence the nodes projecting back to it, recurrent systems appear (**Fig. 2c,**  
121 **d**), which allow activity to dissipate on a much longer time scale. The evoked activity, after the  
122 initial decay, thus persists in the so-called responsive networks (**Fig. 2c, d**), which may reflect  
123 feedback loops and re-entry points in the SC. A dynamically responsive network acts on changes,  
124 for instance, due to sensory stimuli and random fluctuations in the network (flexibility), and  
125 outlasts the stimulation (criticality).

126 The described network properties are illustrated in **Fig. 3a**. The stimulation of three different  
127 areas gives rise to three different responses in a given target area. The differences stem from the  
128 proximity to criticality, which depends upon the SC (in particular the extent of recurrent  
129 networks), comprising the synaptic weights and the time delays (**Fig. 1**). This behavior is  
130 predicted by the center manifold theorem, which is the mathematical basis for criticality (Haken,  
131 1978).

132 *Large-scale brain model.* Dynamics of a vector field  $\Psi(x, t)$  at time  $t \in \mathbf{R}^1$  and position  $x \in \mathbf{R}^3$   
133 in space  $\Omega$  are described by a delay-integro-differential equation:

$$\begin{aligned}
\partial_t \Psi(x, t) = & E(\Psi(x, t)) - a_I I(x, t) \\
& + (1 - \alpha) a_L \int_L dX' \Psi(x - X', t) g(X') \\
& + \alpha a_S \int_L dX' \Psi(x - X', t - \|x - X'\|/\nu) \\
& \times H(X) C(\|x - X'\|/\nu) K^T(X')
\end{aligned} \tag{1}$$

135 were  $\partial_t$  is the derivative with respect to time,  $t$ . The input  $I(x, t)$  allows the stimulation dynamics  
136 to intervene on a node. The operator  $E(\Psi(x, t))$  locally links variables of the vector field. The  
137 scalar  $\alpha$  balances the effect of the homogeneous SC and the heterogeneous SC (first and second  
138 integral) on the vector field. The vectors  $a_I$ ,  $a_L$ , and  $a_S$  of factors relate the input  $I$ , and both types  
139 of SC to the vector field  $\Psi(x, t)$ . The kernel  $g(x)$  describes the homogeneous SC. The field is  
140 time delayed due to a finite transmission speed  $\nu$  via the heterogeneous SC given by matrix  $C(x)$ .  
141 The vectors  $H(x)$  and  $K(x)$  establish the links between the heterogeneous SC and the targets and  
142 the sources. Note that the transmission speed enters the second integral concerning heterogeneous  
143 SC. We assumed the transmission via the homogeneous SC (first integral) to be instantaneous,  
144 which reduces the computational expenses, in order to perform the parameter study. The spatial  
145 and temporal aspects of the model are described in more detail in the following two subsections.  
146 *Geometry and structural connectivity (SC)*. The spatial domain  $\Omega = \{L_1 \cup L_2 \cup S\}$  separates both  
147 cerebral hemispheres  $L = \{L_1 \cup L_2\}$ : left,  $L_1$  and right,  $L_2$ , from subcortical areas  $S$ , that is,  
148  $\cap \Omega = \emptyset$ . A closed 2-sphere describes the geometry of each hemisphere ( $L_1$  and  $L_2$ ). The  
149 homogeneous SC follows a Gaussian distribution  $g(x) = \exp(-x^2 / (2\sigma^2))$  invariant under  
150 translations on  $L$  (Spiegler and Jirsa, 2013). Each closed sphere,  $L_1$  and  $L_2$ , is divided into  $m = 38$   
151 regions, that is,  $L_1 = \cup_{r \in R_1} A_r$  and  $L_2 = \cup_{r \in R_2} A_r$  with  $R_1 = R(m)$ ,  $R_2 = R_1 + n : R(\lambda \in \mathbf{N}) = \{r |$   
152  $r \in \mathbf{N}, r \leq \lambda\}$ , where  $n = 116$  is the number of subcortical areas. The division of the spheres into

153 regions follows a coarser Brodmann map (Kötter and Wanke, 2005) of areas,  $A_r = A(r \in \mathbf{N}) \in \Omega :$   
 154  $\mathbf{N} \rightarrow \mathbf{R}^3$  onto space  $\Omega$  for introducing heterogeneous SC (default model in TVB; Sanz-Leon et  
 155 al., 2013, 2015). The corpus callosum intersects the medial faces of both closed 2-spheres to  
 156 interconnect both cerebral hemispheres from within, leaving two openings. All the nodes in the  
 157 intersecting regions are placed far enough so that the nodes are topologically isolated by  $g(x -$   
 158  $X') \rightarrow 0$ . Finally, one region is the intersection by the corpus callosum and the remaining regions  
 159 are the considered 37 cortical areas composing a cerebral hemisphere. Each of the  $n = 116$   
 160 considered subcortical areas is lumped to a single point in space  $S = \cup_{r \in R_3} A_r$  with  $R_3 = R(n) + 2m$ .  
 161 The heterogeneous connections,  $C$  transmit mean activities of sources to target areas,  $H(x)$  and  $K$   
 162  $(X')$  with a finite transmission speed,  $v = 6 \text{ ms}^{-1}$  (Nunez, 1995, 1981). The square matrix,  $C(\|x -$   
 163  $X'\| / v)$  contains  $(2m + n)^2$  weights,  $c_{ij}(\|x - X'\| / v) : i, j = 1, \dots, 2m + n$  taken from the  
 164 *CoCoMac* database (Kötter et al., 2004, 2005; Stephan et al., 2001) which was extrapolated to  
 165 human (described in Sanz-Leon et al., 2013, 2015). The row vectors  $H(x)$  and  $K(X')$  contain  $2m$   
 166  $+ n$  operations,  $h_i(x)$  and  $k_j(X')$  on the targets and sources, respectively. The operations are  $h_i$   
 167  $(x) = \delta_x(A_i)$  and  $k_j(X') = \delta_{X'}(A_j) / |A_j|$  with the Dirac measure  $\delta_\Omega(A)$  on  $\Omega$  and the cardinality  $|A_r|$   
 168 of the set  $A_r$ .  
 169 The description of the large-scale brain network model (**Eq. 1**) is fully compatible with previous  
 170 TVB descriptions (Sanz-Leon et al., 2015; Spiegler and Jirsa, 2013). Note that the set notation is  
 171 used here to describe brain areas and the division of homogeneously distributed and connected  
 172 network nodes on both cerebral hemispheres into cerebral areas. This is novel here and not  
 173 addressed in previous TVB publications.  
 174 *Temporal dynamics.* The vector field describes a two-dimensional flow (Stefanescu and Jirsa,  
 175 2008) linking two variables  $\Psi(x, t) = (\psi_1 \ \psi_2)^T(x, t)$  in (1) as follows

$$176 \quad E(\Psi(x,t)) = \eta \begin{pmatrix} \psi_2(x,t) - \gamma \psi_1(x,t) - \psi_1^3(x,t) \\ -\varepsilon \psi_1(x,t) \end{pmatrix}. \quad (2)$$

177 The parameterization:  $\gamma = 1.21$  and  $\varepsilon = 12.3083$  sets an isolated brain area close to a critical point,  
 178 that is, an Andronov-Hopf bifurcation (sketched in **Fig. 2**) with a natural frequency around 42 Hz  
 179 using a characteristic rate of  $\eta = 76.74 \text{ s}^{-1}$ . This rhythm in the gamma band accounts for local  
 180 activity such as a coordinated interaction of excitation and inhibition (Buzsáki and Wang, 2012)  
 181 that is not explicitly modeled here. The Dirac delta function is applied to a brain area,  $I_r(x,t) =$   
 182  $-5\eta \delta_x(A_r) \delta(t)$ . The connectivities and the input act on the first variable  $\psi_1(x,t)$  in (1) by  $a_L = a_S$   
 183  $= (a_l)^T = (\eta \ 0)$ . The connectivity-weighted input determines criticality by working against  
 184 inherent energy dissipation (i.e., stable focus) towards the bifurcation. So that the bifurcation was  
 185 not passed, both homogeneous and heterogeneous SC,  $g(x)$  and  $C(\|x - X^*\|/v)$  are normalized  
 186 to unity maximum in-strength across time delays by: (i)  $\int dx g(x) = 1$ , and (ii)

$$187 \quad \sup_{\lambda \in \Omega/v} \left\{ \sum_j^n c_{ij} (|\lambda|) \right\} = 1.$$

188 *Simulation.* To simulate the model on a digital computer, physical space and time are discretized.  
 189 The folding of the human cortex presents a challenge for sampling. The cerebral surfaces,  $L_1$  and  
 190  $L_2$ , are evenly filled with 8,192 nodes. Subcortical structures in  $S$  remain unaffected by the  
 191 discretization. The geometry of the brain is captured in physical space,  $\Omega$  by a net of 16,500  
 192 nodes (i.e. 16,384 cortical and 116 subcortical). The spatial integrals in (1) are rewritten as matrix  
 193 operations, where the heterogeneous SC remains the same and the homogeneous SC is spatially  
 194 sampled on the cerebral surfaces (Spiegler and Jirsa, 2013). The system of difference equations  
 195 are then solved using Heun's method with a time step of 40  $\mu\text{s}$  for 1 second per realization of one  
 196 of the following factors: each of the 190 stimulation sites, SC-balance,  $\alpha = \{0.0, 0.2, 0.4, 0.6, 0.8,$   
 197  $1.0\}$ , and homogeneous spreading,  $\sigma/\text{mm} \in \mathbf{N} : 10 \leq \sigma/\text{mm} \leq 41$ . The implementation is

198 verified by the algebraic solution of an isolated node (i.e., no connections), and by the field  
199 properties (e.g., compact solutions spreading radially around a stimulation site) of the  
200 homogeneously linked cerebral nodes.

201 The lower bound of the spatial range of  $\sigma = 10$  mm results from the used geometrical model for  
202 the cortex. A nearly regular mesh of triangles approximates each cerebral hemisphere with a  
203 finite edge length of 3.9761 mm on average (see Fig.2 and Table 2 in Spiegler and Jirsa, 2013).  
204 The used Gaussian kernel for the homogeneous SC is sampled in the model through the cortical  
205 mesh. Because of the finite edge lengths in the mesh, the spatial range of the homogeneous SC  
206 should not fall below 6.627 mm for  $-3$  dB cutoff of spatial frequencies with respect to their  
207 magnitude (see Tab.7 in Spiegler and Jirsa, 2013). The lower bound of the spatial range of  $\sigma = 10$   
208 mm for the homogeneous Gaussian connectivity kernel causes a loss of at least 20 % of spatial  
209 information (mainly short-range), which corresponds to  $-7.13274$  dB cutoff (see Fig.3 A in  
210 Spiegler and Jirsa, 2013).

211 *Cellular automaton.* The transient period after stimulation onset caused by the transmission times  
212 among the 190 brain areas (74 cortical and 116 subcortical areas) in the heterogeneous SC is  
213 estimated using a cellular automaton. We use the cellular automaton as a tool to determine a time  
214 period for the data decomposition. We focus on the time-delayed interaction among the cerebral  
215 areas in the cellular automaton, because the transmissions via the homogeneous SC (short-range)  
216 of the nodes are instantaneous in the network model in contrast to the heterogeneous SC (long-  
217 range) of areas, which are composed of at least one node. Each of the 190 cells in the cellular  
218 automaton describes one of the brain areas given by the homogeneous SC to be either active or  
219 inactive. The temporal decomposition of the heterogeneous SC according to the transmission  
220 times gives rules for changing the state of cells over time. The cellular automaton is initialized  
221 from the overall inactive state. An activation of a cell triggers a cascade of activation in time until

222 no more cells get activated. In this manner 190 characteristic activation cascades emerged, each  
223 by stimulation, that is, activation of a single cell. The time that the cellular automaton enters the  
224 steady state across all stimulation estimates the transient period from the time delays in the  
225 heterogeneous SC. This estimate of the cellular automaton was then used to set the starting time  
226 for decomposing the simulated data of the full model (Eqs. 1 and 2).

227 *Stimulation and decomposition.* All network nodes of a brain area are constantly stimulated for a  
228 period of the characteristic time of the nodes,  $\eta^{-1}$  to evoke damped oscillations with a maximum  
229 magnitude of one. The stimulation response of an isolated node is subtracted from the response of  
230 stimulated nodes in the network. A *Principal Component Analysis* (PCA) was performed using  
231 the covariance matrix among the 16,500 nodes. The period of 0.5 s data after 0.5 s of stimulus  
232 onset (estimated by the *cellular automaton*) was decomposed. For further analysis, up to three  
233 principal components (i.e., orthogonal) are considered that cover more than 99 % of variance  
234 across conditions.

235 *Subspace similarity, clustering and responsive networks* The dot product of the normalized  
236 eigenvectors from the decomposition the stimulation response was used to measure the similarity  
237 of the dissipation across different stimulation sites for a range of values of the balance of the SC  
238 and a spatial range of the homogeneous SC. The eigenspaces are clustered based on the similarity  
239 measure using k-means for each SC-balance and each range of the homogeneous SC. The number  
240 of clusters is estimated via the gap statistic (Tibshirani et al., 2001). For each cluster, the  
241 eigenspaces are rotated to the basis of the one with the highest similarity among all in the cluster,  
242 using the singular value decomposition and calculating the optimal rotation matrix (Kabsch,  
243 1978). Averaging the aligned basis vectors in a cluster (across eigenspaces) gives the set of  
244 eigenvectors for each cluster. Each resulting eigenvector indicates the contribution of each  
245 network node (e.g., belonging to a cortical or a subcortical structure) to a dynamically responsive



246 network.

247 *Statistics on dynamically responsive networks.* A Kolmogorov-Smirnov test is performed to  
248 determine whether the cortical and the subcortical contributions to a dynamically responsive  
249 network are drawn from the same distribution. A Wilcoxon rank-sum test is used to determine  
250 whether the cortical and the subcortical contributions to a responsive network are equivalent. A  
251 significance level of 0.01 is used for both of these tests.

252 *Comparing dynamically responsive networks and resting state (RS-) networks.* Guided by the  
253 Brodmann area designation of the Automated Anatomical Labeling Template (Tzourio-Mazoyer  
254 et al., 2002) the cartographic description of the RS-networks by Damoiseaux et al. (2006) is  
255 mapped onto the geometrical model of the cortex and its parcellation used here to determine  
256 whether dynamically responsive networks (to stimulation) resemble the experimentally known  
257 spatial activity patterns at rest. In Damoiseaux et al. (2006), cortical structures are either  
258 mentioned or explicitly emphasized to be part of a RS-network, but not explicitly excluded. For  
259 the present purposes, we assumed areas that were not mentioned were also not part of a RS-  
260 network. Finally, in the time since their 2006 publication, there have been a number of updates to  
261 the functional designation of the different RS-networks. We have kept the original designations  
262 save for the ‘unspecified’ RS-network, which seems to best correspond the dorsal attention  
263 network (Cole et al., 2010).

264 The resultant map onto our geometrical model describes the probability of an area to contribute to  
265 a RS-network by three levels: no, medium, or high contribution for unmentioned, mentioned, or  
266 explicitly emphasized in Damoiseaux et al. (2006). The Bhattacharyya coefficient (Bhattacharyya,  
267 1946) is then used to estimate the amount of overlap (i.e., the square root of the inner product)  
268 between a RS- and a dynamically responsive network, which elements are essentially indicated  
269 by an eigenvector. The square of each eigenvector element is taken and summed up within each



270 area. The coarse-grained eigenvectors and each sum of a combination thereof (in total 4) are  
271 normalized to unit length. RS-networks and responsive networks are compared using the  
272 Bhattacharyya coefficient  $BC$  for a RS-network and each normalized coarse-grained eigenvector  
273 or combination thereof. The significance of each comparison,  $p = (n + 1) / (N + 1)$  is estimated by  
274  $N$ -times permuting the entries of a RS-network (without replacement), calculating the coefficient,  
275  $\widetilde{BC}$  (the permuted Bhattacharyya coefficient) and then counting the values greater than the  
276 original,  $n : \widetilde{BC}_i > BC$ , with  $N = 2 \times 10^6$ . The  $p$ -values are corrected due to 24 independent  
277 multiple comparisons (eight RS-networks with three eigenvectors per stimulation site), using the  
278 Bonferroni-Holm-correction. A  $BC$  with  $p$ -values less than 0.05 is considered to be significant.  
279 The mean across the maximum significant overlap for the RS-networks with a responsive  
280 network (i.e., a single eigenvector or a combination thereof) gives the optimal parameters for (i)  
281 the used eigenvector coarsening metric (i.e., absolute or squared value), (ii) the balance of the  
282 homogeneous SC and the heterogeneous SC, and (iii) the spatial range of the homogeneous SC.  
283 The optimum parameter set is separately determined for all the dynamically responsive networks  
284 to cortical, subcortical and both cortical and subcortical stimulations.

285 *Comparing dynamically responsive networks and connectivity structure.* A dynamically  
286 responsive network is measured by means of contributing network nodes after stimulation, that is,  
287 an eigenvector. The spatial structure (in each eigenvector) is specific to each of the dynamically  
288 responsive networks that best explain an experimentally observed RS-network (from **Fig. 4**). The  
289 eigenvectors corresponding to these eight dynamically responsive networks are compared to the  
290 heterogeneous SC. Because this SC describes the wiring between brain areas, the role of each  
291 brain area within the network is characterized using measures from graph theory, namely: in-,  
292 out-, total-degree; in-, out-, total-strength; and clustering coefficient) (Rubinov and Sporns, 2010).  
293 Incoming, outgoing, or all connected ties to an area are measured in terms of (i) their numbers,

294 and (ii) their weights. By counting the connections we obtain the in-, the out-, and the total-  
295 degree. By calculating the sum of connection weights we obtain the in-, the out-, and the total-  
296 strength. The clustering coefficient measures the degree to which areas in a graph tend to group  
297 together. Each of the seven measures of the brain areas in the heterogeneous SC is then compared  
298 with the elements of each dynamically responsive network (i.e., the eigenvector), using the *BC*.  
299 To test statistical significance, the same permutation test is used as for the comparison of the  
300 dynamically responsive networks with the RS-networks.

### Results

301 Following stimulation of a cortical area at rest (i.e., the subcritical regime in **Fig. 2a**, for example,  
302 parameter configuration  $\gamma_1$ ), the induced activity initially spreads radially from the stimulation  
303 site across area boundaries (see, period  $0 < t < 640$  ms in **Fig. 3b**), due to short-range and  
304 homogeneous structural connectivity (SC). Then, propagation occurs across long distances  
305 through the brain network via long-range and heterogeneous SC (see, period  $t \geq 640$  ms in **Fig.**  
306 **3b**), that is, white matter tracts. In contrast to the radial propagation behavior, which is similar for  
307 all cerebral stimulations, non-trivial propagation behavior occurred that is specific to the location  
308 of stimulation. The latter observation can alone be attributed to the weights and time delays of  
309 connections described by the heterogeneous SC (**Fig. 1e**), which forms the propagation in  
310 synergy with the homogeneous SC. Thus, stimulation of adjacent brain areas may cause totally  
311 different propagation patterns, as demonstrated by simulating three different cerebral areas in the  
312 whole-brain model in **Fig. 3b**. Conversely, stimulation at two remote sites may lead to similar  
313 spatiotemporal pattern after an initial transient (see, time frame 890 ms in **Fig. 3b**). We conclude  
314 that the dissipation of the activity induced by stimulation of different sites can resolve in the same  
315 pattern through particular processes formed by the SC. The radial propagation behavior allows  
316 the separation of similar network patterns by their formation starting from different sites.

317 *Dynamically responsive networks.* From the decomposition of the response activity to a particular  
318 stimulation, we obtain three spatially different patterns capturing more than 99 % of the energy  
319 dissipation and describing three dynamically responsive networks per stimulation. Regarding our  
320 parametric study, we find a maximum of eleven different responsive networks across all cerebral  
321 stimulation sites for a ratio of 80 % heterogeneous SC to 20 % homogeneous SC and a spatial  
322 range for homogeneous SC between 30 mm and 35 mm (**Fig. 5a**). Note that the patterns of these  
323 responsive networks are not simply spread activity around the site of stimulation (i.e., radial  
324 propagation). With a network of pure heterogeneous SC, only four responsive networks to  
325 cortical stimulation can be identified; while the number of responsive networks decreases as the  
326 proportion of homogeneous SC increases (**Fig. 5a**). This result supports the synergy of  
327 homogeneous and heterogeneous SC in the formation of the network patterns versus a  
328 predominant formation via heterogeneous SC. We find a maximum of 27 effective stimulation  
329 areas in two occurrences: for a 60 % / 40 % heterogeneous/homogeneous SC-ratio and a spatial  
330 range of 38 mm for the homogeneous SC, and in the case of 100 % heterogeneous SC (**Fig. 5b**).  
331 Note that these are the stimulation of specific cerebral areas that lead to the different responsive  
332 networks, counted in **Fig. 5a**. We conclude that although a pure heterogeneous SC can carry  
333 several dynamically responsive networks, considering homogeneous SC dramatically increases  
334 the repertoire of responsive networks to stimulation. However, there is an optimal value, as too  
335 much homogenous SC is detrimental to the richness of the repertoire.

336 *Dynamically responsive networks and resting state (RS-)networks.* The decomposition of the  
337 response to stimulation of a particular brain area in the whole-brain model resulted in a  
338 description of three responsive networks per stimulation. We thus assessed (i) whether these  
339 functional networks correlate with the experimentally observed RS-networks (Damoiseaux et al.,  
340 2006), and, if so, (ii) whether the set of RS-network patterns do mainly stem from stimulation of

341 specific cortical, subcortical or both brain structures. Interestingly, the optimal ratio of  
342 heterogeneous/homogeneous SC is found to be 20 % / 80 % consistently for all stimulation  
343 conditions. The spatial range for the homogeneous SC is found to be 10 mm for the two groups of  
344 networks responsive to cortical stimulation, and to both stimulation cortical and subcortical. A  
345 spatial range of 17 mm was found to be optimal for the group of networks responsive to  
346 subcortical stimulations. The locations of the stimulation that are most likely to support energy  
347 dissipation into one of the RS-network patterns are listed in **Table 2** (with its corresponding  
348 correlation (Bhattacharyya) coefficient) for each stimulation condition and for the optimal  
349 parameterization. Note that a location may appear repeatedly for the same stimulation condition,  
350 because the activity after stimulation is decomposed into three orthogonal eigenvectors  
351 describing three dynamically responsive networks, where each of which may relate to a different  
352 RS-network (e.g., area AD in thalamus).

353 Irrespective of the restrictions to the stimulation (i.e., cortical, subcortical stimulation and both),  
354 the default mode and the memory network always show the highest correspondence with the  
355 dynamically responsive networks, whereas the visual and the auditory network show the lowest  
356 correspondence (**Table 2**). Moreover, we averaged the best significant coefficients (in **Table 2**)  
357 over the eight RS-networks to assess whether the set of RS-network patterns is driven by (i)  
358 cortical areas, (ii) subcortical areas, or (iii) both cortical and subcortical, where a particular  
359 pattern is either driven cortically or subcortically. Considering the overall correspondence, the set  
360 of RS-network patterns is equally well explained by stimulating subcortical sites ( $\langle BC \rangle = 0.77$   
361 on average) than cortical sites ( $\langle BC \rangle = 0.77$ ), but by stimulating a mixture of both, cortical and  
362 subcortical sites the mean Bhattacharyya coefficient is higher ( $\langle BC \rangle = 0.79$ ). The dynamically  
363 responsive networks matching best with the RS-networks are shown in **Fig. 4**.

364 To assess whether a dynamically responsive network reflects the underlying structure, we  
365 correlated the activity pattern indicating a dynamically responsive network with graph measures  
366 of brain areas in the network of heterogeneous SC (**Figure 6**). Across the different measures, the  
367 in-degree of the SC can be related to the two memory networks and the attention network. For  
368 these RS-networks this means that the in-degree of brain areas given by the SC indicated the  
369 criticality of areas in the operating large-scale brain network model (similar to Kunze et al., 2016),  
370 where criticality is the distance of the operating point of a network node to its inherent  
371 bifurcation.

372 *Stimulation lookup table.* The dynamically responsive networks can be characterized in terms of  
373 stimulation sites, including the responsive networks that resemble RS-network patterns.

374 Assuming a direct link between the spatial activity patterns formed at rest (i.e., RS-networks) and  
375 the task-related functional networks (e.g., related to an external input such as a light flash), RS-  
376 networks can be hence characterized by stimulation of particular structures that can be part of (i)  
377 a network in which information is processed, (ii) an ascending path of sensory input, and (iii)  
378 structures modulating the processing of a certain input (see **Fig.2d**). All stimulation sites for  
379 cortical and subcortical areas of which their responsive networks significantly match with a RS-  
380 network pattern in our model are summarized in **Figure 7**. For example, the pattern for the visual  
381 RS-network is highly responsive to stimulation of the *nucleus geniculatus lateralis thalami* (GL),  
382 which is part of the visual pathway. Considering cortical stimulation, the same pattern is simply  
383 activated by stimulation of the *Gyrus cinguli subgenualis* (CCs), which has been associated to  
384 emotion processing and the pathogenesis of mood disorders (Mayberg et al., 2005). Hence,  
385 stimulation of this cortical area rather modulates information processing in the visual system than  
386 directly affecting the processing such as indicated in **Figure 7a** in the case of the default-mode  
387 and the two memory networks. According to our study of a large-scale whole-brain network

388 model, thalamic stimulations result in activity most prominently in four RS-network patterns:  
389 default mode, motor, working memory and the attention network. Cortical stimulations, in  
390 particular superior temporal, primary motor, secondary visual, and anterior cingulate cortex result  
391 in activity most prominently in the remaining RS-network patterns, namely auditory-  
392 phonological, somato-motor, memory, and ventral stream network. Note that the dynamically  
393 responsive network to cortical areas, especially memory, working memory and somato-motor are  
394 scattered over the cerebral hemispheres (**Fig. 7a**). In addition, **Figure 7** indicates which of the  
395 three responsive networks matches with a RS-network. Considering that the spatial patterns,  
396 which describe the dynamically responsive networks, capture the dissipation of induced network  
397 activity after a specific stimulation (in descending order with the variance), we found the  
398 following RS-network patterns to be dominant (in terms of variance), thus captured in the first  
399 dynamically responsive network: the visual, the auditory, the motor and the working memory  
400 networks. The same is true, to a lesser extent, for the memory, the ventral stream and the  
401 attention network. These RS-networks were represented in the specific second dynamically  
402 responsive network to stimulation, thus weaker (in terms of the variance) of the particular  
403 responses. Interestingly, we found the default mode network to be particularly flexible and  
404 spanned by both the first responsive network and the second responsive network to specific  
405 stimulation.

### **Discussion**

406 This modeling study shows how to generate and predict both spontaneous and task-related  
407 network dynamics. Moreover, it provides an entry point for (i) understanding brain disorders at a  
408 mechanistic level, and (ii) planning more effective therapeutic interventions (i.e., computational  
409 neuropsychiatry, see Deco and Kringelbach, 2014b), for example, through new targets for brain  
410 stimulation. Using a whole-brain model (**Fig. 1**), which is the freely available default large-scale

411 brain network structure of The Virtual Brain ([www.TheVirtualBrain.org](http://www.TheVirtualBrain.org); TVB 1.4.1), we  
412 systematically activated all possible cortical and subcortical areas with brief stimulation to  
413 investigate the brain response as a function of long-range structural connectivity (SC), that is,  
414 white matter fibers, and short-range SC, that is, intracortical connections. We investigated the SC  
415 because information processing in the brain strongly depends upon both short-range  
416 (intracortical) and long-range (intercortical) connections (Deco et al., 2015) and because previous  
417 whole-brain modeling studies mostly focused on long-range SC (Hansen et al., 2015; Deco et al.,  
418 2009, 2011, 2012; Ghosh et al., 2008; Honey et al., 2007). We parametrically varied the ratio of  
419 long-range SC to short-range SC and the spatial range of short-range SC (Spiegler and Jirsa,  
420 2013). We obtained the responsive networks by analyzing the energy dissipation of the stimulus-  
421 induced activity in the full extent of the structural network (**Fig. 3**). The focal activations in the  
422 large-scale brain model may resemble such invasive stimulation techniques as deep brain  
423 stimulation (DBS), for example, single DBS pulse (Montgomery and Gale, 2008; McIntyre et al.,  
424 2004), and such non-invasive techniques as transcranial magnetic stimulation (TMS), for  
425 example, single-pulse and patterned TMS (Dayan et al., 2013). We then contrasted the  
426 dynamically responsive networks to functional networks, more precisely, to the eight  
427 experimentally known resting state (RS-) networks (Damoiseaux et al., 2006). We found that for  
428 a particular configuration of short- and long- SC, the network responds to specific focal  
429 stimulation with activity patterns that closely resemble RS-networks (**Figs. 4,7; Tab. 2**).  
430 Moreover, we found short-range connectivity essential for describing RS-networks.  
431 Mohajerani and colleagues (2013) demonstrated in lightly anesthetized or awake adult mice that a  
432 palette of sensory-evoked and hemisphere-wide activity motifs is represented in spontaneous  
433 activity. Correlation analysis between functional circuits and intracortical axonal projections  
434 indicated a common framework corresponding to long-range monosynaptic connections between



435 cortical areas. Mohajerani et al. (2013) also report that most of the robust activation patterns and  
436 their evolution appeared long after stimulation, reflecting that the initial dynamics are determined  
437 by the local interactions and the stimulation site but the later developments are shaped by the  
438 interplay of connectome and dynamics. These results converge with our findings and suggest that  
439 a polysynaptic connectome shapes the spatiotemporal evolution of spontaneous cortical activity.  
440 In the following, we will discuss the model and the simulation results in more detail.

441 *Large-scale brain network modeling* succeeded under autonomous situations (e.g., driving the  
442 model with noise) to describe the functional connectivity dynamics of ongoing spontaneous brain  
443 activity (Hansen et al., 2015; Deco et al., 2009, 2011, 2012; Ghosh et al., 2008; Honey et al.,  
444 2007). The previous large-scale network model studies mostly considered long-range SC, that is,  
445 white matter tracts. Here, we went beyond this and incorporated short-range SC to understand  
446 how activity propagates and dissipates in the brain (Qubbaj and Jirsa, 2007, 2009; Jirsa, 2004;  
447 Jirsa and Kelso, 2000). Time delays arose from the heterogeneous long-range SC. Due to finite  
448 transmission speeds, time delays in the short-range homogeneous SC may add dynamics to the  
449 network repertoire. The incorporation of these time delays is however challenged by the vast  
450 number of connections (e.g. 40,597,165 connections in our model for a characteristic range of 10  
451 mm of the short-range SC), with that the computational expenses, and is considered for future  
452 work.

453 *Brain dynamics and criticality.* Brain activity and its functional connectivity (FC) are fluctuating  
454 at rest (Allen et al., 2014). FC is thus dynamic and unfolds the SC partially at a given time. To  
455 investigate the dynamically responsive networks to focal stimulation we hypothesized that  
456 networks operate at the brink of criticality. So far, predictions from large-scale brain network  
457 models related to near-criticality have only been tested in autonomous situations of ongoing



458 spontaneous brain activity (Deco et al., 2009, 2011, 2012; Ghosh et al., 2008; Hansen et al.,  
459 2015; Honey et al., 2007). In non-autonomous situations, such as following stimulations of  
460 individual brain areas, (near-)criticality, which is linked mathematically to the local center  
461 manifold theorem (Haken, 1978), predicts that the post-stimulus dynamics evolve with  
462 characteristic features in space and time: (i) the existence of a low-dimensional set of  
463 dynamically responsive networks, and (ii), their slow decay times after stimulation relative to  
464 other networks. This approach provides not only a link between brain stimulation, functionally  
465 relevant networks, and RS-networks (as suggested by Fox et al., 2014), but also gives a better  
466 understanding of the relation between external inputs (e.g., sensory) and internal brain states.

467 We parameterized the model to operate close to criticality (see **Fig. 2**). The criticality in our brain  
468 network model essentially depends on (i) the distance of the node's operating point to the  
469 bifurcation, (ii) the effects of the SC on the nodes' operating point, (iii) the ensemble of signal  
470 transmission delays, and (iv) the stimulation. The model at rest, that is, in absence of external  
471 inputs (i.e., no perturbations such as noise or stimulation) the network model does not show  
472 fluctuations though the SC gives a brain specific topology. Instead, the network is simply silent  
473 without a drive and expresses its activity in virtue of stimulation (processing of inputs) by means  
474 of damped oscillations. At rest, the operating point of each network node is in the same distance  
475 to the critical point, that is, the supercritical Andronov-Hopf bifurcation. Consequently, there is  
476 no activity in the network. An excitatory stimulation pushes the network model closer to  
477 criticality by selectively moving the operating point of particular network nodes closer to the  
478 Andronov-Hopf bifurcation (e.g., from  $\gamma_1$  to  $\gamma_2$  in **Fig. 2a**). Because the stimulation is performed  
479 on brain areas, which are interconnected via the heterogeneous SC, the effect of the stimulation  
480 of the network nodes is particular to the site of stimulation. In this way, we have demonstrated

481 that the dynamically responsive brain networks result from near-criticality and show the most  
482 active and long-lasting patterns following stimulation.

483 *Drivers of brain dynamics* can be internal (i.e., autonomous situation) or external (i.e., non-  
484 autonomous situation). Considering stimulation as driver for brain dynamics, white noise is a  
485 rather unspecific stimulation with respect to time and space as in the autonomous situations  
486 (Deco et al., 2009, 2011, 2012; Ghosh et al., 2008; Hansen et al., 2015). One may however  
487 consider a specific external stimulation (e.g., of a given brain area at a given time) as a particular  
488 realization of a random process at a given time. In this context, it is worth mentioning that the  
489 characteristics of a random process depend on the level of description regarding the SC. For  
490 example, in our cortex model we consider short-range homogeneous SC between adjacent  
491 network nodes and long-range heterogeneous SC between brain areas, which comprise several  
492 nodes (see **Fig. 1**). A spatiotemporally uncorrelated noise added to the state variables on the level  
493 of network nodes will inevitably occur correlated on the level of brain areas. The short-range  
494 homogeneous SC smoothens the spatial variance, and the differential operator smoothens over  
495 time. This indicated that a random process on the level of large-scale brain networks has to be  
496 correlated over space and time. Noise is hence more effective in small structures (e.g., thalamic  
497 nuclei). To determine stochastic processes for driving a model, the spatiotemporal correlations of  
498 brain signals could be used (e.g., see Spiegler and Jirsa, 2013 and the citations therein).

499 *Dynamically responsive networks* are specific to a set of stimulation sites. Activations of a given  
500 brain structure by stimulation leads to a brain response that we characterized by a spatial pattern  
501 of activity. The set of specific activation patterns composes dynamically responsive networks.  
502 Each dynamically responsive network is a *fingerprint* of the network structure given a specific set  
503 of stimulation sites. We extracted the set of dynamically responsive networks by systematically  
504 stimulating the brain areas and then comparing the activity patterns. The responsive networks

505 form a set of different spatial patterns of brain activity, and are specific to a set of stimulation  
506 sites. The meaning of each dynamically responsive network for information processing in the  
507 brain can be discussed with regards to the literature and experimental findings, for example, by  
508 comparing the response networks with the experimentally known RS-networks.

509 *Resting state (RS-) networks* can be characterized by stimulation of particular sites. We  
510 demonstrated that RS-networks could be specifically activated following the stimulation of  
511 specific brain areas. Here, the underlying assumptions are (i) a direct link between the spatial  
512 activity patterns formed at rest, that is, the RS-networks and the task-related functional networks,  
513 and (ii) the emergence of these functional networks from the large-scale brain structure. RS-  
514 networks correlate with functional networks, which are associated during a task with information  
515 processing, such as the perception of a visual stimulus (Damoiseaux et al., 2006). For instance,  
516 the FC of the RS-networks has been correlated with the structural connectivity (SC) of white  
517 matter tracts (van den Heuvel et al., 2009; Greicius et al., 2009; Hermundstad et al., 2013).

518 The RS-networks formed a subset of dynamically responsive networks. In other words, we found  
519 more responsive networks than RS-networks. This indicates that functional networks are not  
520 restricted to the experimentally known RS-networks we considered in this study. These eight RS-  
521 networks were consistent (and showed the least variation around the mean) across ten healthy  
522 subjects (Damoiseaux et al., 2006). This however does not suggest that there are no other, more  
523 variable but stable patterns of activity. For instance, the performance of a perceptual task could  
524 be related to the individual variability in functional connectivity (FC) at rest (Baldassarre et al.,  
525 2012). The way humans approach and perform the same task can be diverse (e.g., Sporns and  
526 Edelman, 1993) and involve a variety of functional processing. The task and its complexity may  
527 concern functional patterns and networks that vary across and within subjects (e.g., on a trial-by-  
528 trial basis). Functional networks are not confined to the experimentally known RS-networks. This

529 applies to dynamically responsive networks in the model with regard to RS-networks also. One  
530 could also argue that brain stimulation (for example, deep brain stimulation) of a particular brain  
531 structure resolves in an activity pattern that is distinct from known (task-related) functional  
532 networks and RS-networks simply because the stimulation directly affects a targeted brain  
533 structure and does not necessarily ascend a sensory pathway (such as a light flash), thus not  
534 processed in (and related to) the known task-related functional networks. Consequently, the  
535 responsive networks that do not match a known functionally related network pattern may reflect:  
536 (i) less dominant/frequent networks, (ii) functional networks that are not directly related to a task  
537 but modulating information processing, or (iii) activation patterns that are specific to direct brain  
538 stimulation. The role of the stimulation site becomes even more apparent from the detailed  
539 analysis of corticocortical SC revealing lateral, ascending and descending projections (Felleman  
540 and Van Essen, 1991), thus a hierarchical organization in which complex interactions, including  
541 feedforward, feedback, and parallel processes are supported (Bressler, 2008). A direct link  
542 between the RS-networks and the task-related functional networks allows the characterization of  
543 RS-networks by the responsiveness to stimulation of particular structures that are part of (i)  
544 networks in which information is processed, (ii) ascending paths of sensory inputs, and (iii)  
545 structures modulating the processing of a certain input (see **Fig.2d**). RS-dynamics originate from  
546 subspaces, in which the ongoing activity evolves and alters, giving rise to non-stationarity as  
547 observed in empirical and computational studies (Allen et al., 2014; Hansen et al., 2015). Our  
548 study predicts that these subspaces can be selectively targeted to bias the brain dynamics towards  
549 the activation of specific functional (task-related) and RS-networks through stimulation of  
550 specific brain areas, for instance, by sensory stimulation (e.g., auditory, visual) and brain  
551 stimulation techniques (e.g., transcranial magnetic stimulation). The stimulation sites are

552 predicted to be network-specific and spatially clustered but distributed (**Fig. 7**). Stimulating  
553 different brain areas could lead to similar activation patterns during rest conditions.

554 *Dynamically responsive networks and the underlying structural connectivity (SC)*. The SC mostly  
555 predict the activity of brain areas directly after stimulation. However, as time evolves, both  
556 implemented types of SC, short-range (homogeneous) SC and large-scale (heterogeneous) SC,  
557 play a crucial role in the spatiotemporal progress. The connectome and its large-scale  
558 heterogeneous SC can explain some, but not all stimulation responsive networks that fit the  
559 experimentally observed RS-networks best (**Fig. 6**). Considering the applied network metrics, it  
560 is interesting to note that the default mode and the memory networks strongly related to the local  
561 embedding of nodes in the topology of the SC, which suggests that they play a special role in  
562 information processing. The activation of the other RS-networks depends to a lesser degree on  
563 the local topologies in the SC and may thus constitute an emergent dynamic process. Emergent  
564 properties can be understood by the transmission and synchronization behavior of the oscillatory  
565 activities throughout the propagation in the network, which decelerates or accelerates the  
566 dissipation process in parts of the network. It has been shown that nodes linked to a network  
567 traverse a node-inherent particular bifurcation (e.g., supercritical Andronov-Hopf bifurcation)  
568 with scaling the connectivity in the order of the in-strength of the nodes in the underlying  
569 structural connectivity (Kunze et al., 2016). This is simply applicable to the two memories and  
570 the attention RS-networks (see **Fig. 6**) in terms of the criticality of nodes, that is, the distance of  
571 the operating point of nodes to its bifurcation point. The comparison with the SC (**Fig. 6**)  
572 indicates that the dissipation processes are sequences of multiple iterations of the SC, thus over  
573 several cycles of damped oscillations, where delays and synchronization naturally play a major  
574 role.

575 Our simulations show that the repertoire of dynamically responsive networks is the richest for the  
576 mixed case in which large-scale heterogeneous and short-range homogeneous SC are  
577 simultaneously present (**Fig. 5**), in keeping with known statistics of synapses within a population,  
578 namely 50 % of intracortical and 50 % of corticocortical fibers (Braitenberg and Schüz, 1998).  
579 The maximum number of different dynamically responsive networks to cerebral stimulation  
580 appeared for a ratio of heterogeneous/homogeneous SC of 60 % / 40 %, where the number of  
581 effective cerebral stimulations is maximum for a ratio of 80 % / 20 %. Interestingly, considering  
582 all stimulation sites, the dynamically responsive networks resembled the RS-networks best for a  
583 different ratio of heterogeneous SC to homogeneous SC, namely of 20 % / 80 % and a spatial  
584 range of the short-range homogeneous SC of 10 mm. The number of different responsive  
585 networks to cerebral stimulation is small (see Fig. 5a), which may indicate the leading role of  
586 thalamic structures at rest and the constrained repertoire of dynamics at rest. The parameter  
587 values for the SC characterized the whole-brain network, thus were similar for all network nodes  
588 and areas, but it is likely that they are brain-area specific (Felleman and Van Essen, 1991).  
589 However, we did not perform an area-specific optimization, as the number of possibilities makes  
590 it computationally intractable at the current time. Furthermore, effects of stimulation on the brain  
591 depend not only on the location of the stimulation, its intensity, its duration, but also on the  
592 dynamical state of the brain (Dayan et al., 2013). Large-scale brain network models could be  
593 used to describe state dependencies of brain responses (e.g., event-related potentials) including  
594 experimental paradigms (e.g., oddball). Not only could the synaptic connections be better adapted  
595 to predict the empirical data, but there are also possibilities for improving the characteristics of  
596 the local dynamics in each brain area. At the moment the regional local dynamics are considered  
597 homogeneous as a matter of simplification, but could be extended to deal with different  
598 heterogeneous local dynamical nodes, for instance, derived from the temporal information in

599 functional data (Deco and Kringelbach, 2014b). Furthermore, the spatial range of the  
600 homogeneous SC was found at the lower boundary of the studied range. Because the lower  
601 boundary depends on the geometrical model of the cortex, a systematic investigation of the  
602 effects of cortex resolution, and with that the approximated homogeneous kernel on large-scale  
603 brain dynamics as suggested by Spiegler and Jirsa (2013) is desirable and crucial for the  
604 incorporation of local and homogeneous SC in a large-scale brain network model.

605 Our model can also be used to study the propagation of hippocampal sharp-wave ripples  
606 (Logothetis et al., 2012) by describing (i) faster and slower rhythms, (ii) the hippocampal  
607 formation (CA1, CA3, dentate gyrus) in more detail (including its specific SC), and (iii) specific  
608 states (e.g., slow-wave sleep and anesthesia). This could provide an entry point for investigating  
609 memory consolidation, changes of brain states, and its functional networks. However, the  
610 stimulation of the hippocampal cortex (HC) activated no RS-networks (**Fig. 7**). This study should  
611 also serve as a good starting point to investigate repetitive stimulation (e.g., with respect to deep  
612 brain stimulation; Murrow, 2014) and the spatiotemporal dynamics of brain resonance  
613 phenomena (see Spiegler et al., 2011).

614 *In conclusion*, we demonstrated that that short-range connectivity proves beneficial in whole-  
615 brain network models for describing brain activity. Moreover, we demonstrated that a large-scale  
616 brain network dissipate their energy spatiotemporally upon stimulation in a characteristic low-  
617 dimensional manner, which is consistent with the idea that the brain operates close to criticality.  
618 The stimulation responsive networks are compatible with the empirically known RS-networks  
619 and are set apart by the slow time scale as predicted by theorems of near-criticality. Stimulation  
620 sites can be assembled in topological groups that approximate empirical RS-networks. A  
621 stimulation of brain areas in these groups predicts an evolution of the RS-dynamics towards  
622 lower-dimensional subspaces, in which the subsequent dynamics evolve and can be characterized

623 by conventional functional connectivity (FC) approaches. Our results suggest a means to bias RS-  
624 dynamics via spatially coordinated stimulation towards target subspaces. Given that FC of the RS  
625 differentiates groups with different pathologies and across ages, our results are of interest for  
626 approaches of such brain stimulation techniques as transcranial electrical stimulation, transcranial  
627 magnetic stimulation, and deep brain stimulation directed towards therapy and cognitive  
628 enhancement.



## References

- 629 Allen EA, Damaraju E, Plis SM, Erhardt EB, Eichele T, Calhoun VD (2014) Tracking whole-  
630 brain connectivity dynamics in the resting state. *Cereb Cortex* 24:663-76.
- 631 Baldassarre A, Lewis CM, Committeri G, Snyder AZ, Romani GL, Corbetta M (2012) Individual  
632 variability in functional connectivity predicts performance of a perceptual task. *Proc Natl*  
633 *Acad Sci USA* 109: 3516-21.
- 634 Bhattacharyya A (1946) On a measure of divergence between two multinomial populations.  
635 *Sankhya* 7:401-6.
- 636 Braitenberg V, Schüz A (1998) *Cortex: Statistics and geometry of neuronal connectivity*.  
637 Springer (Berlin Heidelberg).
- 638 Braitenberg, V, Schüz, A (1991) *Anatomy of the cortex: statistics and geometry*. Springer (Berlin  
639 Heidelberg).
- 640 Bressler (2008) Neurocognitive networks. *Scholarpedia* 3:1567.
- 641 Buzsáki G, Wang XJ (2012) Mechanisms of gamma oscillations. *Annu Rev Neurosci* 35:203-25.
- 642 Cole DM, Smith SM, Beckmann CF (2010) Advances and pitfalls in the analysis and  
643 interpretation of resting-state fMRI data. *Front Syst Neurosci* 4:8.
- 644 Damoiseaux JS, Rombouts SARB, Barkhof F, Scheltens P, Stam CJ, Smith SM, Beckmann CF  
645 (2006) Consistent resting-state networks across healthy subjects. *Proc Natl Acad Sci USA*  
646 103:13848-53.
- 647 Dayan E, Censor N, Buch ER, Sandrini M, Cohen LG (2013) Noninvasive brain stimulation:  
648 from physiology to network dynamics and back. *Nat Neurosci* 16:838-44.
- 649 Deco G, Tononi G, Boly M, Kringelbach, ML (2015) Rethinking segregation and integration:  
650 contributions of whole-brain modeling. *Nat Rev Neurosci* 16:430-9.
- 651 Deco G, McIntosh AR, Shen K, Hutchison RM, Menon RS, Everling S, Hagmann P, Jirsa VK

- 652 (2014a) Identification of optimal structural connectivity using functional connectivity and  
653 neural modeling. *J Neurosci* 34:7910-6
- 654 Deco G, Kringelbach M (2014b) Great expectations: using whole-brain computational  
655 connectomics for understanding neuropsychiatric disorders. *Neuron* 84:892-905.
- 656 Deco G, Jirsa VK, McIntosh AR (2013) Resting brains never rest: computational insights into  
657 potential cognitive architectures. *Trends Neurosci* 36:268-74.
- 658 Deco G, Jirsa VK (2012) Ongoing cortical activity at rest: Criticality, multistability, and ghost  
659 attractors. *J Neurosci* 32:3366-75.
- 660 Deco G, Jirsa VK, McIntosh AR (2011) Emerging concepts for the dynamical organization of  
661 resting-state activity in the brain. *Nat Rev Neurosci* 12:43-56.
- 662 Deco G, Jirsa V, McIntosh AR, Sporns O, Kötter R (2009) Key role of coupling, delay, and noise  
663 in resting brain fluctuations. *Proc Natl Acad Sci USA* 106:10302-7.
- 664 Felleman DJ, Van Essen DC (1991) Distributed hierarchical processing in the primate cerebral  
665 cortex. *Cereb Cortex* 1:1-47.
- 666 Fox MD, Buckner RL, Liu H, Chakravarty MM, Lozano AM, Pascual-Leone A (2014) Resting-  
667 state networks link invasive and noninvasive brain stimulation across diverse psychiatric and  
668 neurological diseases. *Proc Natl Acad Sci USA* 111:E4367-75.
- 669 Ghosh A, Rho Y, McIntosh AR, Kötter R, Jirsa VK (2008) Noise during rest enables the  
670 exploration of the brain's dynamic repertoire. *PLoS Comput Biol* 4:e1000196.
- 671 Greicius MD, Supekar K, Menon V, Dougherty RF (2009) Resting-state functional connectivity  
672 reflects structural connectivity in the default mode network. *Cereb Cortex* 19:72-8.
- 673 Haken H (1978) *Synergetics: An introduction nonequilibrium phase transitions and self-*  
674 *organization in physics, chemistry and biology.* Springer (Berlin Heidelberg).
- 675 Hansen EC, Battaglia D, Spiegler A, Deco G, Jirsa VK (2015) Functional connectivity dynamics:

- 676 Modeling the switching behavior of the resting state. *Neuroimage* 105:525-35.
- 677 Hermundstad AM, Bassett DS, Brown KS, Aminoff EM, Clewett D, Freeman S, Frithsen A,  
678 Johnson A, Tipper CM, Miller MB, Grafton ST, Carlson JM (2013) Structural foundations of  
679 resting-state and task-based functional connectivity in the human brain. *Proc Natl Acad Sci*  
680 USA 110:6169-74.
- 681 Honey CJ, Kötter R, Breakspear M, Sporns O (2007) Network structure of cerebral cortex shapes  
682 functional connectivity on multiple time scales. *Proc Natl Acad Sci USA* 104:10240-5.
- 683 Jirsa VK (2004) Connectivity and dynamics of neural information processing. *Neuroinformatics*  
684 2:183-204.
- 685 Jirsa VK, Kelso JAS (2000) Spatiotemporal pattern formation in neural systems with  
686 heterogeneous connection topologies. *Phys Rev E* 62:8462-5.
- 687 Kabsch W (1978) A discussion of the solution for the best rotation to relate two sets of vectors.  
688 *Acta Crystallogr Sect A* 34:827-8.
- 689 Kötter R, Wanke E (2005) Mapping brains without coordinates. *Phil Trans R Soc B* 360:751-66.
- 690 Kötter R (2004) Online retrieval, processing, and visualization of primate connectivity data from  
691 the cocomac database. *Neuroinformatics* 2:127-44.
- 692 Kunze T, Hunold A, Haueisen J, Jirsa V, Spiegler A (2016) Transcranial direct current  
693 stimulation changes resting state functional connectivity: A large-scale brain network  
694 modeling study. *Neuroimage* S1053-8119(16)00122-1.
- 695 Logothetis NK, Eschenko O, Murayama Y, Augath M, Steudel T, Evrard HC, Besserve M,  
696 Oeltermann A (2013) Hippocampal-cortical interaction during periods of subcortical silence.  
697 *Nature* 491:547-53.
- 698 Mayberg HS, Lozano AM, Voon V, McNeely HE, Seminowicz D, Hamani C, Schwab JM,  
699 Kennedy SH (2005) Deep brain stimulation for treatment-resistant depression. *Neuron* 45:651-

700 60.

701 McIntyre CC, Savasta M, Kerkerian-Le Goff L, Vitek JL (2004) Uncovering the mechanism(s) of  
702 action of deep brain stimulation: activation, inhibition, or both. *Clin Neurophysiol* 115:1239-  
703 48.

704 Mohajerani MH, Chan AW, Mohsenvand M, LeDue J, Liu R, McVea DA, Boyd JD, Wang YT,  
705 Reimers M, Murphy TH (2013) Spontaneous cortical activity alternates between motifs  
706 defined by regional axonal projections. *Nat Neurosci* 16:1426-35.

707 Montgomery EB Jr, Gale JT (2008) Mechanisms of action of deep brain stimulation (DBS).  
708 *Neurosci Biobehav Rev* 32:388-407.

709 Murrow RW (2014) Penfield's prediction: a mechanism for deep brain stimulation. *Front Neurol*  
710 5:213.

711 Nunez PL (1995) *Neocortical dynamics and human EEG rhythms*. Oxford Univ Press.

712 Nunez PL (1981) *Electric fields of the brain*. Oxford Univ Press.

713 Qubbaj MR, Jirsa VK (2009) Neural field dynamics under variation of local and global  
714 connectivity and finite transmission speed. *Physica D*, 238:2331-46

715 Qubbaj MR, Jirsa VK (2007) Neural field dynamics with heterogeneous connection topology.  
716 *Phys Rev Lett* 98:238102.

717 Rubinov M, Sporns O (2010) Complex network measures of brain connectivity: uses and  
718 interpretations. *Neuroimage* 52:1059-69.

719 Sanz-Leon P, Knock SA, Spiegler A, Jirsa VK (2015) Mathematical framework for large-scale  
720 brain network modeling in the virtual brain. *Neuroimage* 111:385–430.

721 Sanz-Leon P, Knock SA, Woodman MM, Domide L, Mersmann J, McIntosh AR, Jirsa V (2013)  
722 The virtual brain: a simulator of primate brain network dynamics. *Front Neuroinform* 7.

723 Shew WL, Plenz D (2013) The functional benefits of criticality in the cortex. *Neuroscientist*

- 724 19:88-100.
- 725 Spiegler A, Jirsa V (2013) Systematic approximations of neural fields through networks of neural  
726 masses in the virtual brain. *Neuroimage* 83:704-25.
- 727 Spiegler A, Knösche TR, Schwab K, Haueisen J, Atay FM (2011) Modeling Brain Resonance  
728 Phenomena Using a Neural Mass Model. *PLoS Comput Biol* 7:e1002298.
- 729 Sporns O, Edelman GM (1993) Solving Bernstein's problem: a proposal for the development of  
730 coordinated movement by selection. *Child Dev* 64:960-81.
- 731 Stefanescu RA, Jirsa VK (2008) A low dimensional description of globally coupled  
732 heterogeneous neural networks of excitatory and inhibitory neurons. *PLoS Comput Biol*  
733 4:e1000219.
- 734 Stephan KE, Kamper L, Bozkurt A, Burns GAPC, Young MP, Kötter R (2001) Advanced  
735 database methodology for the collation of connectivity data on the macaque brain (CoCoMac).  
736 *Phil Trans R Soc B* 356:1159-86.
- 737 Tibshirani R, Walther G, Hastie T (2001) Estimating the number of clusters in a data set via the  
738 gap statistic. *J R Stat Soc* 63:411-23.
- 739 Tzourio-Mazoyer N, Landeau B, Papathanassiou D, Crivello F, Etard O, Delcroix N, Mazoyer B,  
740 Joliot M (2002) Automated Anatomical Labeling of Activations in SPM Using a Macroscopic  
741 Anatomical Parcellation of the MNI MRI Single-Subject Brain. *Neuroimage* 15:273-89.
- 742 van den Heuvel MP, Mandl RC, Kahn RS, Hulshoff Pol HE (2009) Functionally linked resting-  
743 state networks reflect the underlying structural connectivity architecture of the human brain.  
744 *Hum Brain Mapp* 30:3127-41.

## Figures and tables

745 **Figure 1.** Structure of the large-scale brain model. The large-scale brain model is composed of  
746 (a) the brain's geometry of 116 subcortical areas and the two cerebral hemispheres. There are 37  
747 cortical areas (b), each containing between 29 and 683 nodes (dots in (a)), for a total of 8,192  
748 nodes per hemisphere. (c) Homogenous and heterogeneous structural connectivity (SC).  
749 Heterogeneous SC corresponds to white matter tracts connecting brain areas over long distances.  
750 Homogenous SC corresponds to gray matter fibers, with short-range connections within a given  
751 area, but also enabling some communication over short distances between neighboring areas.  
752 Although Area 2 is not connected to Areas 1 and 3 via the white matter, it is weakly linked to  
753 both areas via a set of short-range SC. (d) Homogeneous SC matrix for the 16,384 nodes. The  
754 synaptic weights are color-coded. The diagonal describes in warm colors the strong SC of  
755 adjacent nodes. SC decreases with distance, which is shown in cold colors. SC of nearby nodes  
756 are scattered (e.g., blue dots) in (d) because each cerebral hemisphere is described by a surface,  
757 which makes it impossible to cluster nodes locally along both axes. Note the absence on  
758 interhemispheric short-range SC. (e) Heterogeneous SC for the 190 (74 cortical + 116  
759 subcortical) areas for weights (left panel) and time delays (right panel). Within one hemisphere,  
760 the 58 subcortical areas mostly project to the 37 cortical ones. Some connections between  
761 subcortical areas can also be seen. The 37 cortical areas project heavily to both cortical and  
762 subcortical areas. Some interhemispheric connections can also be seen. Note also the presence  
763 of large time delays.

764 **Figure 2.** The large-scale brain model works near criticality. **(a)** Each node in the model is  
765 parameterized by  $\gamma$  to operate intrinsically at the same distance from the critical point if  
766 unconnected. A node shows zero activity or oscillation ( $\sim 42$  Hz) in response to stimulation (red  
767 crosses). The activity at each node is described by two time-dependent variables,  $\psi_1(t)$  and  $\psi_2(t)$ .  
768 The closer a node operates to the critical point, the larger and the longer lasting is the oscillation  
769 (compare  $\gamma_1$  and  $\gamma_2$ ). When the critical point is reached, the node intrinsically performs a rhythm  
770 of constant magnitude. The model, however, is set so that the critical point is never exceeded. **(b)**  
771 Principles of activity spreading after stimulation. The damped oscillation generated in the  
772 stimulated node (1) is sent via its efferent connections to its target node (2), triggering there, in  
773 turn, a damped oscillation with weaker amplitude and faster decay, which then propagates to the  
774 next node. Activity  $\psi_1^{(j)}(t)$  of node ( $j$ ) is scaled by  $c_{ij}$  and transmitted to node ( $i$ ) via homogeneous  
775 and heterogeneous connections (SC), delayed by  $\tau_{ij}$  in the latter case. In such a chain, activity  
776 would decay fast. **(c)** In the large-scale brain model, multiple activity re-entry points can be found.  
777 At any time point, the dynamics of a node is influenced by all incoming activity. The node's  
778 response to stimulation (1) is relayed to linked nodes (2-4), which may be fed back to (1) via (4)  
779 and may allow the induced activity to dissipate on a much longer time scale. The network  
780 response thus depends upon the SC and allows the network to operate near criticality. **(d)**  
781 Activation of dynamically responsive networks. Activity after stimulating a node (1 or 2) in a  
782 series connection decays fast (as in **b**). However, activity may circulate and thus decays slower in  
783 a feedback network (4-5). Such remaining activity after the initial stimulation decay reveals the  
784 so-called dynamically responsive networks.

785 **Figure 3.** Dissipation after stimulation. **(a)** Response of area PFCcl to the activation of three  
786 different regions PMCdl, CCp and PCm (abbreviations are given in **Table 1**). Note that the  
787 amplitude, decay and phase of the response depend upon the stimulated area. The main  
788 determinants of the response pattern are the connections, the synaptic weights and the time delays.  
789 The envelope of the time series is computed (black, gray and green lines for the three stimulation  
790 sites). **(b)** Spatiotemporal activation following stimulation of three different regions. At a given  
791 time point, we extract the amplitude of the envelope for the 16,500 nodes (the 16,384 cortical  
792 nodes and the 116 subcortical ones), which we normalize to 1. The color scale thus indicates the  
793 contribution of a given region to the overall activity. The dissipation of activity after stimulating  
794 two distant brain areas, PMCdl and CCp (located far from one another: PMCdl in the lateral  
795 surface, CCp in the medial surface) leads to similar topographical patterns (for  $t > 640$  ms). In  
796 contrast, a distinct pattern appears when stimulating PCm, which is adjacent to CCp. **(c)**  
797 Extraction of the main activated propagation subnetworks. We use the stimulation of PMCdl as  
798 an example. We calculate the covariance among the 16,500 time series (the 16,384 cortical nodes  
799 and the 116 subcortical ones) for a time window centered at 750 ms and then perform a Principal  
800 Component Analysis (PCA) to extract the subnetworks capturing >99 % of the activity. Three  
801 different networks are thus dynamically responsive when PMCdl is stimulated.



802 **Figure 4** Comparison between dynamically responsive networks to stimulation (top rows) and  
803 the experimentally observed RS-networks (bottom rows) for the lateral and medial surface of the  
804 brain. From **a–h**: default mode, visual, auditory-phonological, somato-motor, memory, ventral-  
805 stream, dorsal attention and working memory. We used 20 % / 80 % for the ratio of  
806 heterogeneous/homogeneous SC and a range of 10 mm for the homogeneous SC. The white to  
807 red scale gives the relative contribution of areas to the responsive networks (top rows) and the  
808 RS-networks (bottom rows). The stimulation sites are given in **Table 2** and **Fig. 7**. Note that the  
809 bottom rows are activity masks for the 74 cortical areas constituting the RS-networks, where  
810 activity is not localized within areas and uniformly color-coded (see Materials and Methods). The  
811 top rows show the vector field  $\Psi(x, t)$  on the mesh of 16,384 cortical nodes and thus localized  
812 activity.

813 **Figure 5** Repertoire of dynamically responsive networks. **(a)** The number of networks responsive  
814 to cerebral stimulation depends on the spatial range of the homogeneous SC and the ratio of  
815 homogeneous SC to heterogeneous SC. Similar in **(b)** for the number of effective cerebral  
816 stimulation sites leading to different networks.

817 **Figure 6** Influence of the structure on the RS-like networks. The pattern of each stimulation  
818 responsive network (from **Fig. 5**) that best explains an experimentally observed RS-network  
819 (rows) is correlated with the underlying heterogeneous SC using seven graph-theoretic measures  
820 (columns). Incoming, outgoing, or all connected ties to an area can be measured in terms of  
821 number, i.e., in-, out-, total-degree, or in terms of strength, i.e., in-, out-, total-strength. The  
822 clustering coefficient measures the degree to which areas in a graph tend to cluster together. *BC*  
823 indicates a matching with warmer colors, where comparisons marked with a star are statistically  
824 significant. Note that correlations may be high but not significant using a permutation test. The  
825 in-degree of the heterogeneous SC can be related to the two memory networks and the attention  
826 network. The activation of the other RS-networks emerges in a way that is not predicted by the  
827 network metrics.

828 **Figure 7** RS-like networks triggered by stimulation. Cortical stimulations in **a**, and subcortical in  
829 **b** lead to dynamically responsive networks correlating significantly with RS-networks for a ratio  
830 of 20 % / 80 % of the heterogeneous/homogeneous SC and a range of 10 mm of the  
831 homogeneous SC.  $BC = [0, 1]$  indicates a matching with higher values. The eigenvectors,  $EV$  (1  
832 to 3 in descending order of eigenvalues and captured variance), indicate the responsive  
833 network(s) to an effective stimulation matching with RS-networks. Abbreviations are listed in  
834 **Table 1**. Note that the sites triggering a particular pattern can be scattered over the cerebral  
835 hemispheres (e.g., for the two memory networks and the somato-motor network).

836 **Table 1** Abbreviations of brain areas. Number of nodes per cortical areas in brackets (left, right).

A1	Primary auditory cortex (57,74)	Cld	Capsule of the nucleus lateralis dorsalis
A2	Secondary auditory cortex (33,64)	CnMd	Nucleus centrum medianum thalami
Amyg	Amygdala (151,135)	Cs	Nucleus centralis superior thalami
CCa	Gyrus cinguli anterior (54,49)	Csl	Nucleus centralis superior lateralis thalami
CCp	Gyrus cinguli posterior (167,179)	GL	Nucleus geniculatus lateralis thalami
CCr	Gyrus cinguli retrosplenialis (68,67)	GM	Nucleus geniculatus medialis thalami
CCs	Gyrus cinguli subgenualis (29,42)	GMpc	Nucleus geniculatus medialis thalami, pars parvocellularis
FEF	Frontal eye field (104,161)	IL	Intralaminar nuclei of the thalamus
G	Gustatory cortex (52,42)	LD	Laterodorsal nucleus (thalamus)
HC	Hippocampal cortex (75,54)	Li	Nucleus limitans thalami
Ia	Anterior insula (48,71)	LP	Nucleus lateralis posterior thalami
Ip	Posterior insula (82,111)	MD	Nucleus medialis dorsalis thalami
M1	Primary motor area (463,460)	MDdc	Nucleus medialis dorsalis thalami, pars densocellularis
PCi	Inferior parietal cortex (454,371)	MDmc	Nucleus medialis dorsalis thalami, pars magnocellularis
PCip	Cortex of the intraparietal sulcus (355,486)	MDmf	Nucleus medialis dorsalis thalami, pars multiformis
PCm	Medial parietal cortex (196,241)	MDpc	Nucleus medialis dorsalis thalami, pars parvocellularis
PCs	Superior parietal cortex (199,177)	ML	Midline nuclei of the thalamus
PFCcl	Centrolateral prefrontal cortex (328,227)	Pa	Nucleus paraventricularis thalami
PFCdl	Dorsolateral prefrontal cortex (248,216)	Pac	Nucleus paraventricularis caudalis thalami
PFCdm	Dorsomedial prefrontal cortex (211,270)	Pen	Nucleus paracentralis thalami
PFCm	Medial prefrontal cortex (61,68)	Pf	Nucleus parafascicularis thalami
PFCorb	Orbital prefrontal cortex (310,265)	PT	Nucleus parataenialis thalami
PFCpol	Pole of prefrontal cortex (279,279)	Pul	Nucleus pulvinaris thalami
PFCvl	Ventrolateral prefrontal cortex (380,479)	Pul.i	Nucleus pulvinaris inferior thalami

PHC	Parahippocampal cortex (267,212)	IPul.l	Nucleus pulvinaris lateralis thalami
PMCdl	Dorsolateral premotor cortex (108,138)	Pul.m	Nucleus pulvinaris medialis thalami
PMCm	Medial premotor cortex (149,68)	Pul.o	Nucleus pulvinaris oralis thalami
PMCVl	Ventrolateral premotor cortex (126,138)	R	Nucleus reticularis thalami
S1	Primary somatosensory cortex (487,420)	Re	Nucleus reuniens thalami
S2	Secondary somatosensory cortex (107,116)	SG	Nucleus suprageniculatus thalami
TCc	Central temporal cortex (436,422)	Teg.a	Nucleus tegmentalis anterior
TCi	Inferior temporal cortex (390,306)	VA	ventral anterior nucleus (thalamus)
TCpol	Pole of temporal cortex (91,101)	VAmc	Nucleus ventralis anterior thalami, pars magnocellularis
TCs	Superior temporal cortex (306,352)	VAPc	Nucleus ventralis anterior thalami, pars parvocellularis
TCv	Ventral temporal cortex (260,317)	VL	ventral lateral nucleus (thalamus)
V1	Visual area 1 (147,180)	VLc	Nucleus ventralis lateralis thalami, pars caudalis
V2	Secondary visual cortex (683,663)	VLM	Nucleus ventralis lateralis thalami, pars medialis
AD	Nucleus anterior dorsalis thalami	VLo	Nucleus ventralis lateralis thalami, pars oralis
AM	Nucleus anterior medialis thalami	VLps	Nucleus ventralis lateralis thalami, pars postrema
AN	Anterior nuclei of the thalamus	VP	Nucleus ventralis posterior
AV	Nucleus anterior ventralis thalami	VPI	Nucleus ventralis posterior inferior thalami
Caud	Nucleus caudatus	VPL	Aentral posterior lateral nucleus (thalamus)
Cdc	Nucleus centralis densocellularis thalami	VPLc	Nucleus ventralis posterior lateralis thalami, pars caudalis
Cif	Nucleus centralis inferior thalami	VPLo	Nucleus ventralis posterior lateralis thalami, pars oralis
Cim	Nucleus centralis intermedialis thalami	VPM	Nucleus ventralis posterior medialis thalami
Cl	Nucleus centralis lateralis thalami	VPMpc	Nucleus ventralis posterior medialis, pars parvocellularis
Clau	Clastrum	X	Area X (thalamus)
Clc	Nucleus centralis latocellularis thalami		

---

837 **Table 2** The stimulation sites corresponding to the dynamically responsive network that best  
 838 match a particular RS-network. All responsive networks of a parameter configuration were  
 839 compared to the eight experimentally known RS-networks. A permutation test was performed to  
 840 test the significance of each comparison. The multiple comparisons were corrected using the  
 841 Bonferroni-Holm-correction. For the comparison, the dynamically responsive networks were  
 842 differentiated into: cortically, subcortically responsive networks, and the union of all responsive  
 843 networks irrespective of the stimulation site. For each of these three groups separately, the  
 844 parameterization was found to show the best accordance of stimulation responsive networks with  
 845 the entire set of RS-networks. The optimal parameterization is the ratio of 20 % / 80 % for the  
 846 heterogeneous/homogeneous SC and the range of 10 mm for the homogeneous SC for all groups,  
 847 except the range is with 17 mm different for the group of responsive networks to subcortical  
 848 stimulation. Note the presence of cortical and subcortical sites in the last column, which has  
 849 higher matching values on average over the eight RS-networks compared to the other groups. The  
 850 value in parenthesis is the matching coefficient (it varies between 0 and 1). Abbreviations are  
 851 listed in **Table 1**.

Resting state network	Stimulation condition		
	Cortex (excl. subcortex)	Subcortex (excl. cortex)	Cortex and Subcortex
Default mode	PFCm (0.8337)	AD (0.8420)	AD (0.8506)
Visual	CCs (0.6455)	GL (0.6953)	GL (0.7510)
Auditory-phonological	TCs (0.7147)	GMPC (0.6630)	TCs (0.7147)
Somato-motor	M1 (0.8153)	MDDC (0.8199)	M1 (0.8153)
Memory	V2 (0.8646)	MDDC (0.8454)	V2 (0.8646)
Ventral stream	CCa (0.7845)	ML, AN, SG (0.8122)	CCa (0.7845)
Dorsal attention	M1 (0.7039)	R, VA, X (0.7097)	AD (0.7631)

Working memory

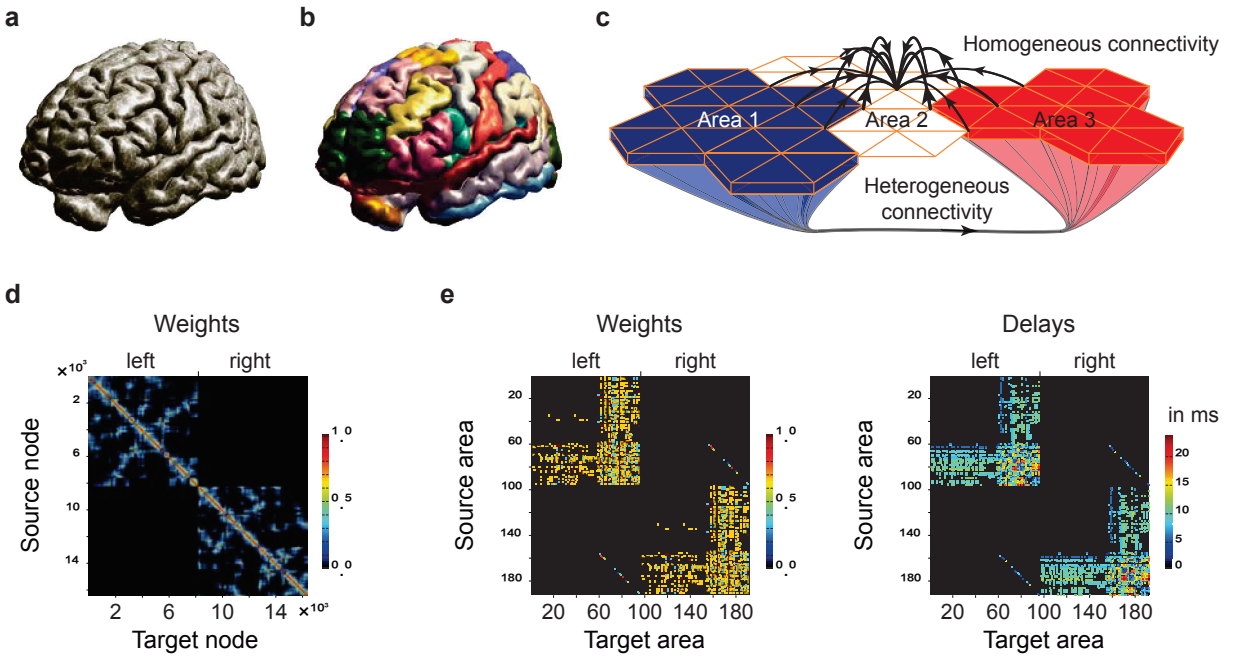
CCs (0.8006)

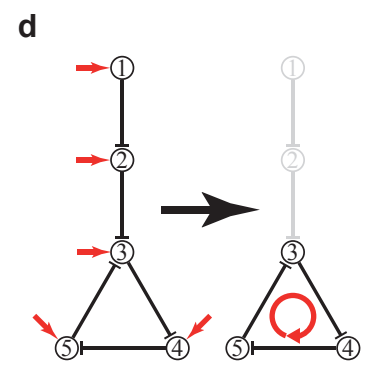
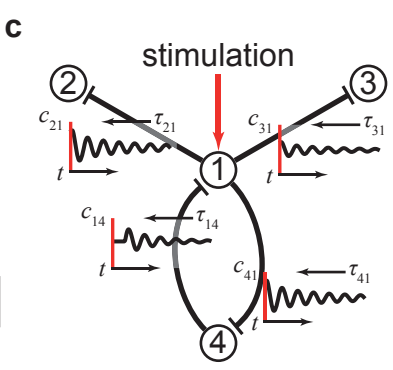
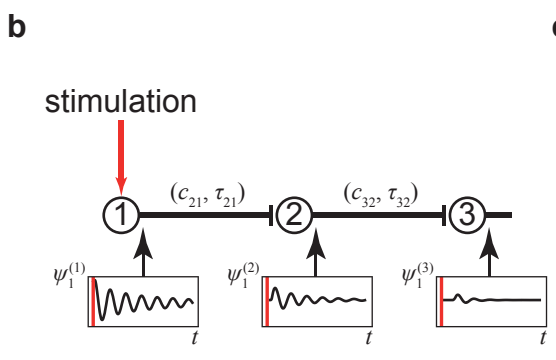
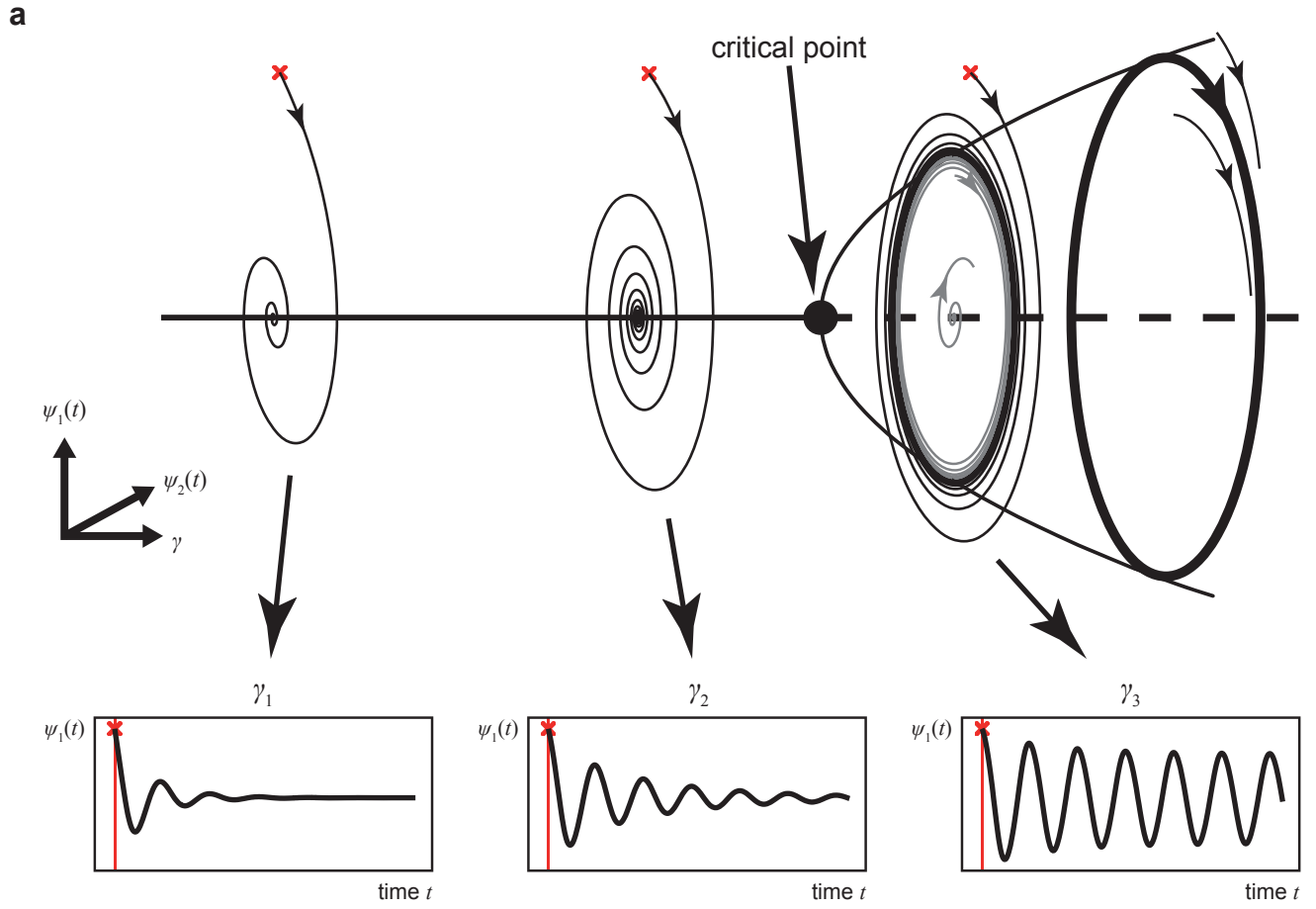
PAC, Cdc (0.8204)

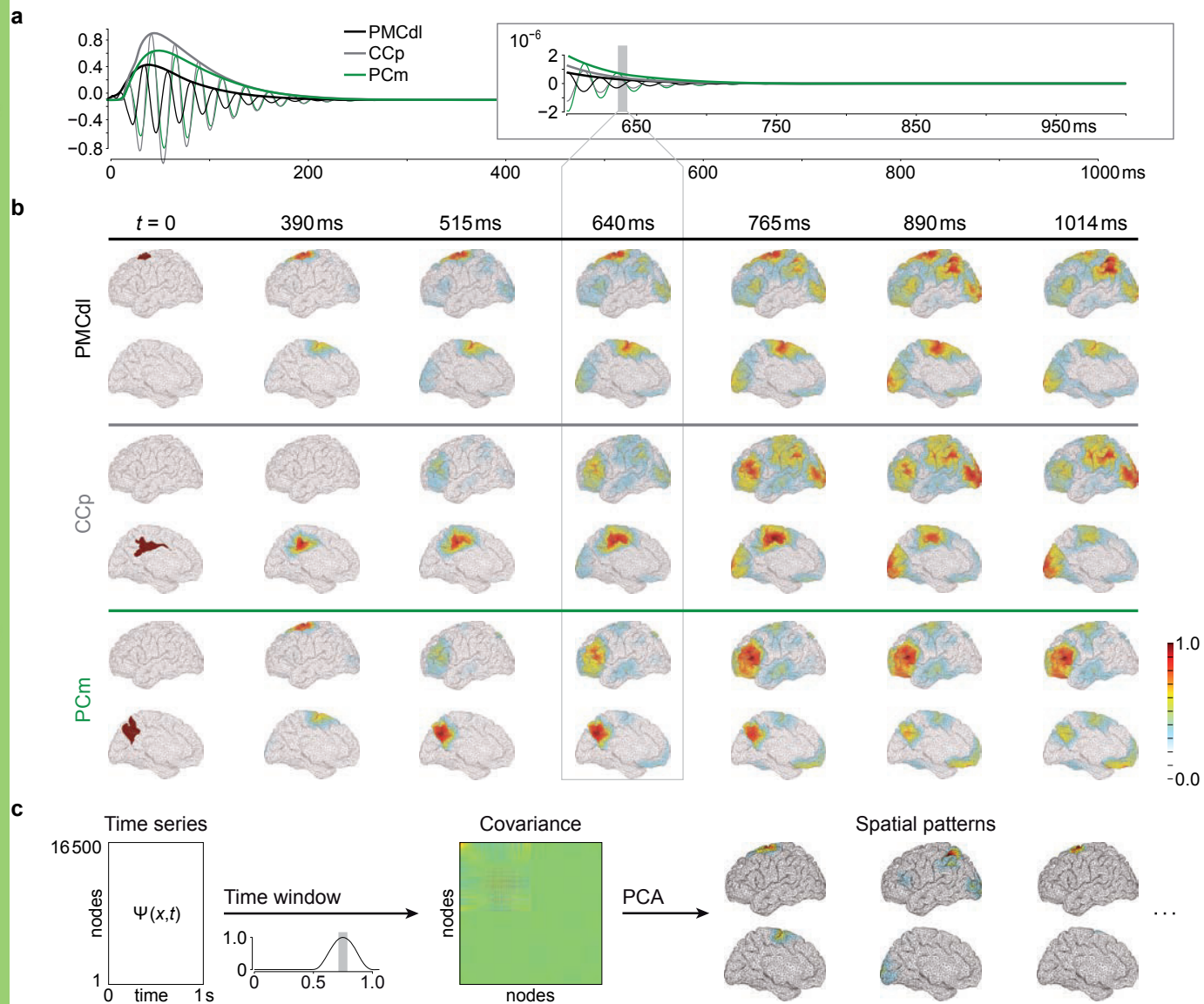
GL (0.8069)

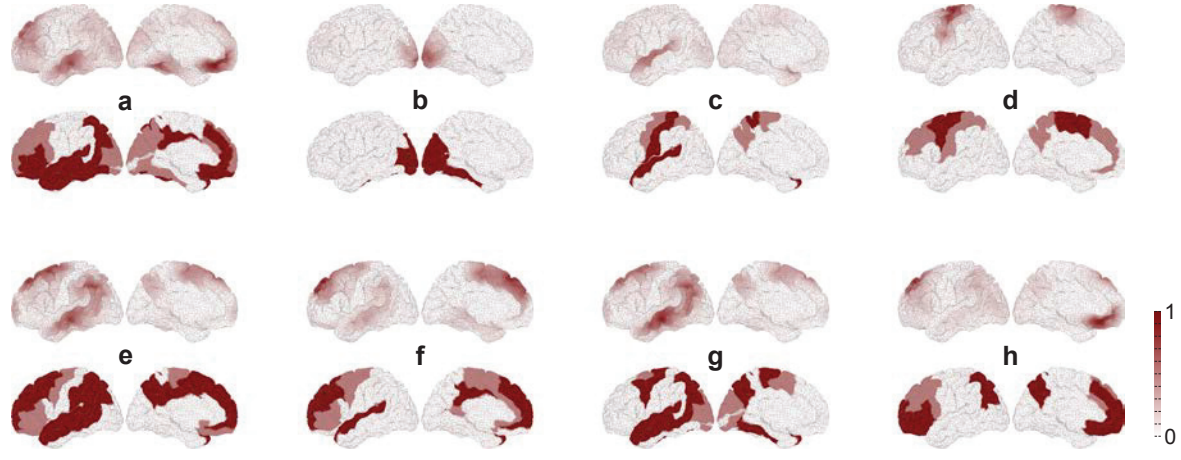
---

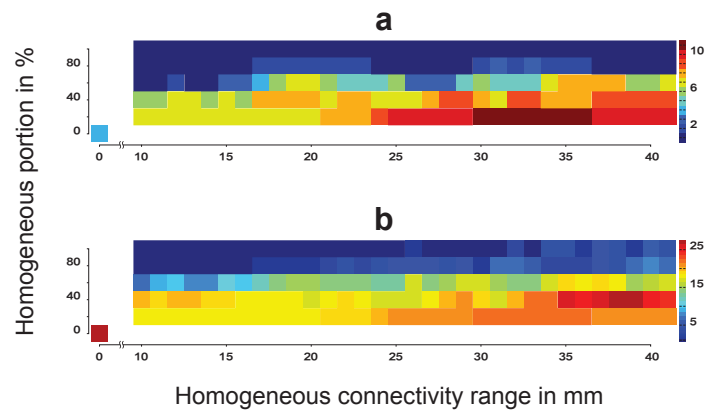


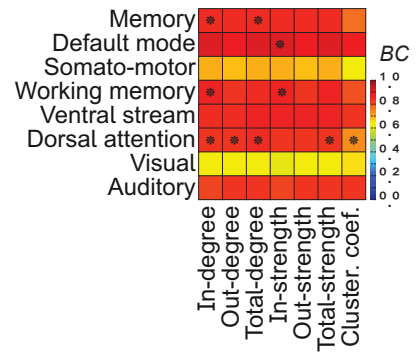




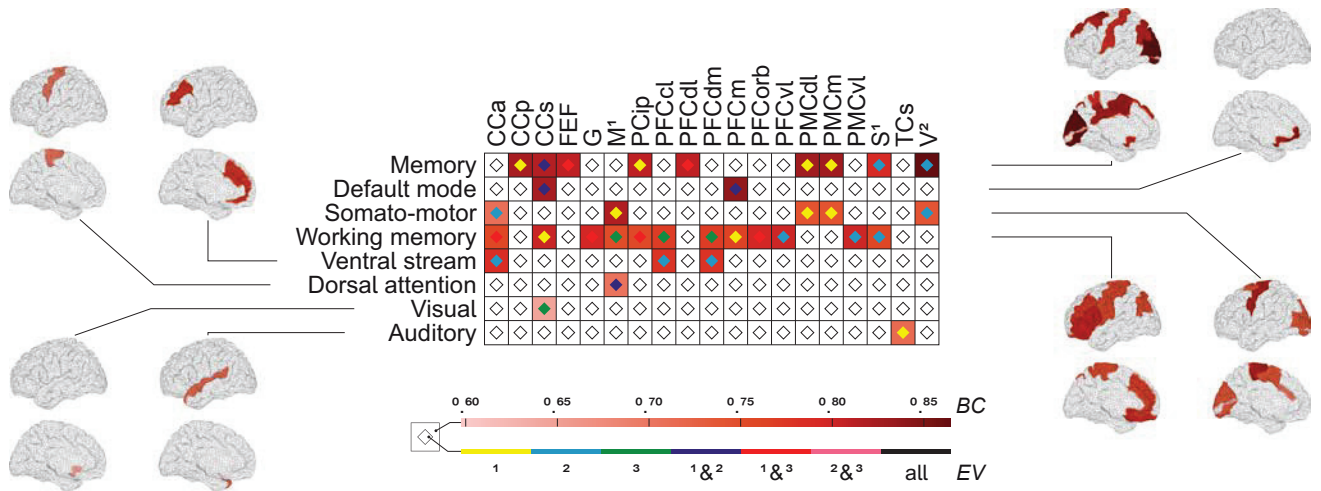








a



b

